Analytical Methods

ROYAL SOCIETY OF CHEMISTRY

PAPER

View Article Online
View Journal | View Issue

Cite this: *Anal. Methods*, 2021, **13**, 1238

Theoretical and experimental verification of imaging resolution factors in scanning electrochemical microscopy†

Qiang Xiong, Tao Wu, Ranran Song, Fan Zhang * and Pingang He*

Received 6th January 2021
Accepted 15th February 2021

DOI: 10.1039/d1ay00025j

rsc.li/methods

The imaging resolution of scanning electrochemical microscopy (SECM) depends strongly on the tip electrode size and the tip–substrate distance. Herein, etched glass encapsulation was applied to fabricate a gold disk electrode, and the size of the tip electrode was accurately determined from the steady-state limiting current. Referring to the theoretical research carried out by our predecessors, the formula for the imaging resolution was derived, followed by the imaging of gold spots and cells with the prepared microelectrodes of different sizes and with different tip–substrate distances. A depth scan was performed to generate 2D current maps of the gold spot relative to the position of the microelectrode in the x–z plane. Probe approach curves and horizontal sweeps were obtained from one depth scan image by simply extracting vertical and horizontal cross-sectional lines, and further characterized by comparison with simulated curves through modeling of the experimental system. The experimental results were basically consistent with the theory, revealing that the highest imaging resolution can be obtained with the smallest tip electrode when $d/a = 1$, and when the size of the tip electrode is fixed the smallest tip–substrate distance can give the highest imaging resolution.

Introduction

Scanning electrochemical microscopy (SECM) is a type of scanning probe microscope technique proposed by Allen Joseph Bard in the late 1980s.[1,2] Engstrom's group also made important contributions to the invention of SECM, using microelectrode probes to monitor the spatial distribution of electrode products.[3] Due to the chemical sensitivity of SECM, it can not only characterize the surface morphology of conductors and insulators, but also distinguish the electrochemical activity of the substrate surface to study the biomolecules and cells fixed on the substrate that can produce electroactive substances or have their own electric charge. SECM is commonly used for chemical kinetics studies,[4–6] microfabrications,[7] electrochemical imaging,[8–11] the effect assessment of drugs on cells[12–14] and neurotransmitter release,[15,16] and accurate localized analysis of complex substrates.[17–19]

As it is an imaging technique, resolution is very important for SECM. Thus, it is particularly necessary to study how to improve the resolution. As the inventor of SECM, Allen Joseph Bard had done a lot of research on the theory of resolution under different working modes of SECM.[20–22] In the feedback mode, a straightforward and established theoretical method, proposed by Bard's group, can be used to calculate the variation of the normalized tip current with the tip–substrate distance. They found that for conductive substrates, the tip current was a function of tip–substrate distance, while for insulating substrates, the tip current was both dependent upon d and the insulating sheath radius.[20] It was found that a smaller tip–substrate distance could increase the resolution of substrates and could be used to improve the SECM resolution.[21] In order to illustrate the effect of tip size on SECM resolution, an interdigitated array electrode was scanned with electrodes of different sizes. It was found that higher resolution was obtained with smaller electrodes.[22] Zhifeng Ding's group also investigated the effect of scanning distance on imaging resolution, revealing that a smaller electrode-to-sample distance during the horizontal sweep could generate a higher resolution for the transition region of the substrate.[23] Consequently, the tip–substrate distance and the size of the tip electrode have been proven to affect the imaging resolution in the feedback mode through different experiments, but the imaging resolution has not been mathematically described up to now. Christine Lefrou carried out similar research, deriving formulae for positive and negative feedback currents relative to tip size, tip–substrate distance, and R_G value, but did not go much further to find the relationship between the resolution and tip current.[24–26] SECM imaging resolution has often been mentioned in the literature, but there is no accurate definition, and the

School of Chemistry and Molecular Engineering, East China Normal University, 500 Dongchuan Road, Shanghai 200241, P. R. China. E-mail: fzhang@chem.ecnu.edu.cn; pghe@chem.ecnu.edu.cn; Fax: +86-21-54340049; +86-21-54340057; Tel: +86-21-54340049; +86-21-54340057

† Electronic supplementary information (ESI) available: MatLab calculation code; schematic illustration of the fabrication of Au disk electrodes; cyclic voltammetry experiments; SEM images. See DOI: 10.1039/d1ay00025j

dependence of SECM resolution on experimental parameters has not been described. Therefore, it is necessary to use a mathematical formula to describe the SECM image resolution, which will be helpful in guiding researchers to obtain the optimal image resolution in experiments.

Herein, in order to study the factors that affect the SECM imaging resolution, the feedback mode is employed, which is the most important mode in SECM imaging. Using the SECM feedback mode to detect biological samples, positive and negative feedback current regions could appear due to the influence of sample morphology and the nature of the substrate. When both conductive and insulating domains of a sample are significantly larger than the tip electrode, the current of the tip electrode on the conductor and the insulator could satisfy the formulae for positive and negative feedback currents, respectively.[18,24,25] Therefore, based on the positive and negative feedback current formulae, the mathematical expression for the real-time current of the SECM tip and the imaging resolution has been derived, which reveals the effects of tip electrode size and tip–substrate distance on imaging resolution. The accuracy of the imaging resolution formula was verified by scanning the regular gold spots at different tip–substrate distances using tip electrodes of different sizes. The obtained results were in good agreement with the simulation results obtained using the formula, verifying that the imaging resolution was indeed related to the tip electrode size and the tip–substrate distance. We proved that when the size of the tip electrode is fixed, reducing the tip–substrate distance can improve the imaging resolution. In addition, during the experiment, in order not to damage the sample, a certain distance needs to be maintained between the tip electrode and the sample. The choice of the tip electrode is not the smaller the better, but to choose a tip electrode with a size equivalent to the tip–substrate distance to get the best imaging resolution. This work provides theoretical support and guidance to improve the imaging resolution in SECM feedback mode.

Theory

SECM images are actually obtained with the feedback current generated at the tip electrode due to the different characteristics of substrates. Therefore, in order to study the factors influencing the SECM imaging resolution, the feedback current change of the tip electrode on substrates with different properties first needs to be explored. According to the theory of Allen Joseph Bard,[18] for the feedback mode, both the tip electrode and the substrate were immersed in a solution containing electrolyte and a redox species (*e.g.*, a reducible species, O). This species can be reduced at the tip electrode, and the product, R, can be reoxidized at the substrate:

$$\mathrm{O} + n\mathrm{e}^- \rightarrow \mathrm{R}\ \text{(on the tip electrode)} \quad (1)$$

$$\mathrm{R} - n\mathrm{e}^- \rightarrow \mathrm{O}\ \text{(on the substrate)} \quad (2)$$

The rate of reduction reaction on the tip electrode is controlled by the rate of O diffusion to the tip electrode, when the tip electrode is far from the substrate. Thus, the steady-state diffusion current on the tip electrode can be expressed by the following formula:[18,27]

$$i_{\mathrm{T},\infty} = 4nDFac \quad (3)$$

where $i_{\mathrm{T},\infty}$ is the steady-state diffusion limiting current, n is the number of transferred electrons, D is the diffusion coefficient of O, F is the Faraday constant, a is the radius of the tip electrode, and c is the bulk concentration of the redox species.

As the tip electrode gets closer to the substrate, the current i_{T} of the tip electrode changes with the properties of the substrate. A normalized tip current, I_{T}, is defined as the ratio of tip electrode current near the substrate (i_{T}) to the tip electrode current at an infinite distance from the substrate ($i_{\mathrm{T},\infty}$):[24]

$$I_{\mathrm{T}} = \frac{i_{\mathrm{T}}}{i_{\mathrm{T},\infty}} \quad (4)$$

When the substrate is a conductor, the R generated on the tip electrode can diffuse to the substrate and be oxidized to O, followed by the diffusion of O to the tip electrode to be reduced. This formed loop could increase the reduction current of the tip electrode, which is called positive feedback with $I_{\mathrm{T}} > 1$, defined as $I_{\mathrm{T}}^{\mathrm{c}}$. When the substrate is an insulator, the generated R cannot be re-oxidized at the substrate. Meanwhile, as the tip electrode approaches the substrate, it hinders the diffusion of O from the bulk solution to the tip, leading to the decline of tip electrode current with the decrease of distance. This is called negative feedback with $I_{\mathrm{T}} < 1$, defined as $I_{\mathrm{T}}^{\mathrm{i}}$.

When the tip electrode scans the boundary of a sample with an insulator and conductor, the tip electrode current is affected by both negative feedback current and positive feedback current. Therefore, I_{T} can be expressed as formula (5):

$$I_{\mathrm{T}} = kI_{\mathrm{T}}^{\mathrm{i}} + (1 - k)I_{\mathrm{T}}^{\mathrm{c}} \quad (5)$$

where k is the coefficient representing the influence of negative feedback current on tip electrode current.

When the distance between the tip electrode and the sample is very small, when the tip electrode is above the insulator the tip electrode current presents completely negative feedback and will not be affected by the conductor. In this case, $k = 1$ in formula (5). When the tip electrode is above the conductor the current presents completely positive feedback and will not be affected by the insulator, giving $k = 0$. When the tip electrode is at the edge of the insulator and conductor, the current of the tip electrode will change sharply from negative feedback current to positive feedback current (or from positive feedback current to negative feedback current) as the tip electrode scans the boundary from the insulator to the conductor (or from the conductor to the insulator). However, because the area of the tip electrode and the distance between the tip electrode and the sample cannot be infinitely small, the boundary current diffusion described in formula (5) will result in the blurring and broadening of the boundary between the insulator and conductor.[32] Therefore, the broadening is equal to twice the radius of the tip electrode, represented by $2a$.

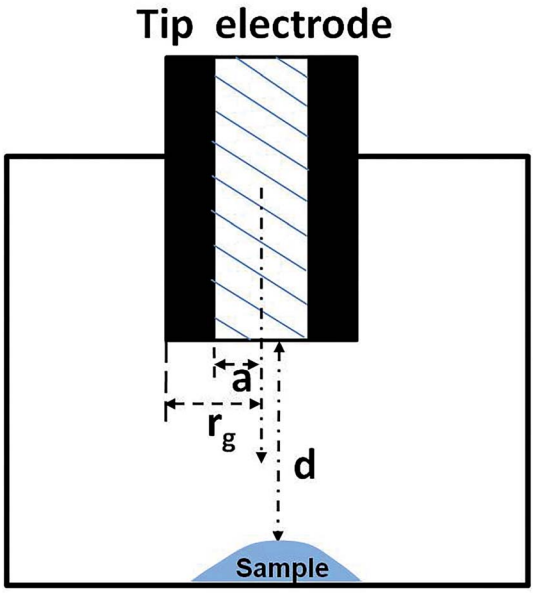

Scheme 1 A diagram of the cross-sectional view of a tip electrode in solution.

On the other hand, the imaging resolution is positively related to the difference between the pure positive and negative feedback currents, which is reflected in the contrast of the image. That is to say, a more obvious imaging contrast can be generated by a larger current difference.[23,32] Therefore, the imaging contrast can be expressed as $I_T^c - I_T^i$.

In feedback mode, the imaging resolution of SECM is related to both broadening and imaging contrast, presenting directly and inversely proportional correlations, respectively. Because the image broadening is $2a$ and the imaging contrast is $I_T^c - I_T^i$, the imaging resolution (IR) of SECM can be presented as formula (6), showing that better imaging resolution with smaller IR can be obtained with smaller broadening and greater contrast. This definition expresses the effect of broadening and imaging contrast on IR, so that the factors affecting IR can be further analyzed and verified.

$$\mathrm{IR} = \frac{2a}{I_T^c - I_T^i} \tag{6}$$

For positive feedback, there are various mathematical formulae to describe the effect on I_T^c.[18,25,29] A simple analytical expression is shown in formula (7):[28,29]

$$I_T^c = 0.68 + \frac{0.78377}{\frac{d}{a}} + 0.3315 \exp\left(\frac{-1.0672}{\frac{d}{a}}\right) \tag{7}$$

where d is the tip–substrate distance, and a is the radius of the tip electrode. For negative feedback, I_T^i can be expressed as formula (8):[18,24]

$$I_T^i = \frac{\frac{2.08}{R_G^{0.358}}\left(\frac{d}{a} - \frac{0.145}{R_G}\right) + 1.585}{\frac{2.08}{R_G^{0.358}}\left(\frac{d}{a} + 0.0023R_G\right) + 1.57 + \frac{\ln R_G}{\frac{d}{a}} + \frac{2}{\pi R_G}\ln\left(1 + \frac{\pi R_G}{2\frac{d}{a}}\right)} \tag{8}$$

The R_G value will have a greater influence on the shape of the current–distance curve; therefore, its effect should be considered. R_G equals r_g/a, where r_g is the radius of the insulating sheath (Scheme 1).

The imaging resolution formula can be obtained by substituting formulae (7) and (8) into (6), as shown in formula (S1) in the ESI.† After ignoring the less influential algebraic expressions, the formula for imaging resolution is simplified to formula (9):

$$\mathrm{IR} = \frac{\mathrm{d}R_G^{0.36}\left[3.14\pi\frac{d}{a}R_G + 2\pi R_G \ln R_G + 4.16\pi\left(\frac{d}{a}\right)^2 R_G^{0.64} + 4\frac{d}{a}\ln\left(1 + \frac{\pi R_G}{2\frac{d}{a}}\right)\right]}{\left[\pi R_G^{1.36}\ln R_G + 2\frac{d}{a}R_G^{0.36}\ln\left(1 + \frac{\pi R_G}{2\frac{d}{a}}\right)\right] \times \left[0.68\frac{d}{a} + 0.33\frac{d}{a}\exp\left(\frac{-1.0672}{\frac{d}{a}}\right) + 0.78\right] + 0.30\pi\left(\frac{d}{a}\right)^2 + \pi\frac{d}{a}R_G^{1.36}\left[-0.52\frac{d}{a} + 0.52\frac{d}{a}\exp\left(\frac{-1.0672}{\frac{d}{a}}\right) + 1.23\right] + \pi\left(\frac{d}{a}\right)^2 R_G\left[-0.67\frac{d}{a} + 0.69\frac{d}{a}\exp\left(\frac{-1.0672}{\frac{d}{a}}\right) + 1.63\right]} \tag{9}$$

where IR is the imaging resolution, d is the tip–substrate distance, a is the radius of the tip electrode, and R_G equals r_g/a. The unit of IR can be denoted by μm. Clearly, a smaller value of IR indicates a higher imaging resolution.

When the radius of the tip electrode tends to be infinitely small, this transition region also tends to zero, and the tip electrode current directly changes from negative feedback current to positive feedback current, indicating that the

imaging is consistent with the actual features, and the broadening is zero. It increases as the size of the electrode increases. When the radius of the tip electrode is constant, the broadening does not change. Decreasing the tip–substrate distance produces a sharper contrast between the negative and positive feedback currents. When the tip–substrate distance is constant, the contrast becomes smaller due to the smaller radius of the tip electrode. Therefore, the imaging resolution is related to d and a.

In order to clarify the factors affecting the imaging resolution, formula (9) is discussed. Obviously, the IR value is related to the size of the tip electrode, the tip–substrate distance, and the R_G value. When R_G is a constant, IR depends on two variables: a, the radius of the tip electrode, and d, the tip–substrate distance. When a is a constant, IR has a definite function relationship with d. Similarly, a fixed value of d can generate a definite function relationship of IR with a. Thus, the effects of a and d on IR to obtain the minimum value are discussed using the control variable method.

By substituting a certain R_G value and different d values into formula (9), the function relationship between IR and a can be obtained. Fig. 1A shows this relationship when $R_G = 10$ and $d =$ 3, 5 or 10 μm, respectively. It is found that if d equals 3 μm, IR is minimized when a is 3 μm. Similarly, the same conclusions could be reached with $d = 5$ μm and $d = 10$ μm, revealing that when d is a constant, IR is the minimum when the values of a and d are equal, not when a is the smallest. Matlab software is used to program formula (9) to obtain the minimum IR. The calculation code is shown in formula (S2).† It could also be found that when $d/a = 1$, the IR value reaches its minimum, giving the highest imaging resolution. Clearly, the two methods lead to the same conclusion that when d is a constant, the minimum IR is obtained by keeping the size of the tip electrode and the tip–substrate distance equal.

In the same way, the function relationship between IR and d can be obtained according to formula (9) when a is fixed. Fig. 1B exhibits this relationship when $R_G = 10$ and $a = 3$, 5 or 10 μm, respectively, showing that a smaller IR is generated with a smaller tip–substrate distance, when fixing the size of the tip electrode.

In summary, if the tip–substrate distance is determined, a tip electrode with a size equivalent to the tip–substrate distance should be selected to get the minimum IR. On the other hand, for a certain size tip electrode, a smaller tip–substrate distance can contribute to a smaller IR. This means that the highest imaging resolution can be obtained with the smallest tip electrode when $d/a = 1$, and when the size of the tip electrode is fixed the smallest tip–substrate distance can also give the highest imaging resolution. This work provides guidance for the optimal choice of experimental conditions for SECM imaging.

Experimental section

Reagents and instruments

Gold wires with diameters of 25 μm and 1 mm were purchased from Alfa Aesar. Borosilicate capillaries (1 mm outer diameter and 0.75 mm inner diameter) were obtained from Sutter Instrument Co. Hydrogen chloride (36.0–38.0% HCl) and epoxy resin were purchased from Sinopharm Chemical Reagent Co. Ltd. All the solid reagents, including potassium ferricyanide ($K_3Fe(CN)_6$, AR), ferrocenemethanol (FMA), potassium chloride (KCl, AR), ethanol (AR), sodium hydroxide (NaOH, AR), concentrated nitric acid (HNO_3, AR, 98%), hydrogen peroxide (H_2O_2, 30%), and ferrocene (Fc, AR) were weighed on an analytical balance. The liquid reagents and solutions were transferred with a pipette. All the aqueous solutions were prepared from secondary ultrapure water (18 MΩ cm).

The scanning electrochemical microscope CHI 920C (CH Instruments, Austin, TX, USA) and electrochemical workstations were from Shanghai CH Instruments. The P-2000 laser puller was from Sutter Instrument Company, USA. The electrode etching experiment was performed on the electrochemical workstation CHI820B. Electrochemical data were collected on the electrochemical workstation CHI820B.

The low range and high range representations of the electrode surface topography were obtained on an Olympus Corporation Optical Microscope (Olympus-CX31 system microscope) and scanning electron microscope (SEM, Hitachi S-4800, Tokyo, Japan), respectively.

Fabrication of Au disk electrodes

The Au disk electrodes were fabricated by a two-step process (Fig. S1†). As shown, in step 1, a gold wire 1 cm in length and 25

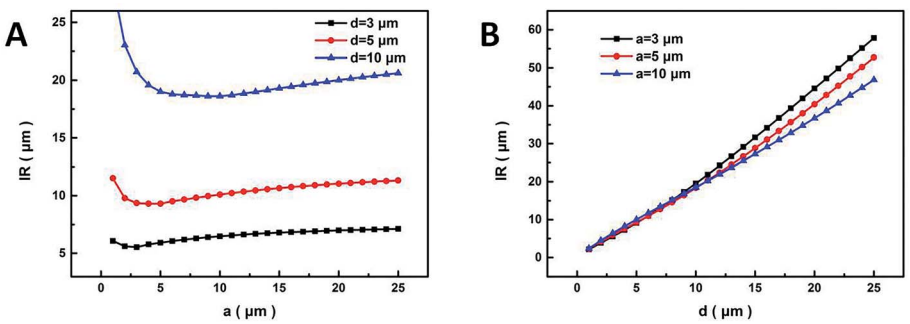

Fig. 1 (A) Function relationship between IR and the size of the tip electrode when d is 3 μm, 5 μm and 10 μm; (B) function relationship between IR and the tip–substrate distance when a is 3 μm, 5 μm and 10 μm.

μm in diameter was connected to a copper wire with silver epoxy and put in an oven at 100 °C for 1 h. A micropipette was pulled from a borosilicate capillary using a laser puller. The 5 pulling parameters are as follows: heat = 450, filament = 3, velocity = 40, delay = 100 and pull = 220. Then, the gold wire was carefully inserted from the end of the glass tube and extended 0.5 cm outside the tube. Then, it was slowly immersed into a mixed solution of HCl : H_2O = 3 : 7 (volume ratio) vertically. The gold wire was etched using amperometry at 2.2 V with a gold ring electrode as the counter electrode and a Ag/AgCl electrode as the reference electrode, following the adjustment of its location to face the right core of the gold ring. The gold wire etching time was 10 s. Afterwards, the etched gold wire was cleaned with water and ethanol, and dried in air. With the help of the microscope, it was carefully pulled back close to the glass tube and an appropriate amount of epoxy resin was injected for encapsulation. Then, the glass tube was heated at 120 °C for 1 h to solidify the epoxy resin. The encapsulation and the location of the gold wire in the glass tube were verified using the microscope. Finally, the gold wire was polished by the fine sandpaper fixed on an ultramicroelectrode polisher (step 2) until the appearance of an S-shaped curve.

Imaging of gold spots

Gold spots 50 μm in diameter deposited on an insulating silicon wafer were imaged using the fabricated Au disk electrodes with radii of 12.00 μm, 2.23 μm and 0.76 μm using a CHI 920C scanning electrochemical microscope in 0.5 mM FMA with a Ag/AgCl electrode as a reference electrode, and Pt wire as a counter electrode. All the measurements were performed at room temperature.

Cell imaging

Human breast cancer cells (MCF-7) were acquired from the Chinese Academy of Sciences (Shanghai, China). They were cultured in a humidified incubator at 37 °C with 5% CO_2. For SECM measurements, MCF-7 cells were plated in glassy Petri dishes and the culture medium was changed to 0.5 mM FMA prior to SECM scanning. A single cell was positioned under the microscope. Then, a Au disk electrode with the application of a constant potential was employed for cell scanning, while recording the current signals.

Results and discussion

Characterization of the Au disk electrodes

Cyclic voltammetry (CV), scanning electron microscopy (SEM), and SECM approach curves were employed to characterize the Au disk electrodes, including the size, the quality of the sealing and polishing and the R_G value.

The effective radius (R_{eff}) of the Au disk electrodes (Fig. S2†) can be estimated by measuring the steady-state diffusion limiting current (formula (3)).[30] According to Bard's theory, formula (3) only applies to $R_G \approx 10$. So, constant "4" in formula (3) was adjusted by a suitable value for a given R_G, for example, 4.06 ($R_G = 10$), 4.43 ($R_G = 2$), and 4.64 ($R_G = 1.5$).[18]

When performing the measurement in 10 mM $K_3Fe(CN)_6$ solution (0.5 M KCl solution as a supporting electrolyte), the values of the steady-state limiting current and the corresponding R_{eff} of the tip electrode are as listed in Table S1,† according to its diffusion coefficient $D = 7.2 \times 10^{-6}$ cm^2 s^{-1}, the Faraday constant $F = 96\,485$ C mol^{-1}, and concentration $C = 10$ mM.

The double-layer charging current and the characteristic peaks for steady-state diffusion exhibited by the cyclic voltammetry curves indicate the quality of the sealing and polishing. The shape of the tip electrode, and the quality of the sealing and polishing can be clearly shown by a SEM image (Fig. S3†). The R_G value can be calculated from the ratio of insulating glass sheath radius to conductive Au wire radius.

Effect of tip electrode radius on the IR of SECM

In order to verify the accuracy of the factors affecting the imaging resolution of SECM, a 2 × 2 gold spot array 50 μm in diameter and 100 nm in thickness was prepared on an insulating silicon wafer (Fig. 2) and imaged by three tips with radii of 12.00 μm, 2.23 μm and 0.76 μm, keeping $d/a = 1$, respectively.

The horizontal sweeps across the gold spot were performed in 0.1 M KCl containing 0.5 mM FMA solution with holding the tip potential at +0.45 V for electrochemical oxidation of FMA. The SECM responses depended on the surface conductivity. A positive feedback was observed ($i_T > i_{T,\infty}$) when the tip was over the gold spot, due to the regeneration of FMA at the conducting substrate. When the tip passed over the insulating part, no regeneration of FMA resulted in a negative feedback ($i_T < i_{T,\infty}$). When the tip electrode scans the gold spot, the current depends

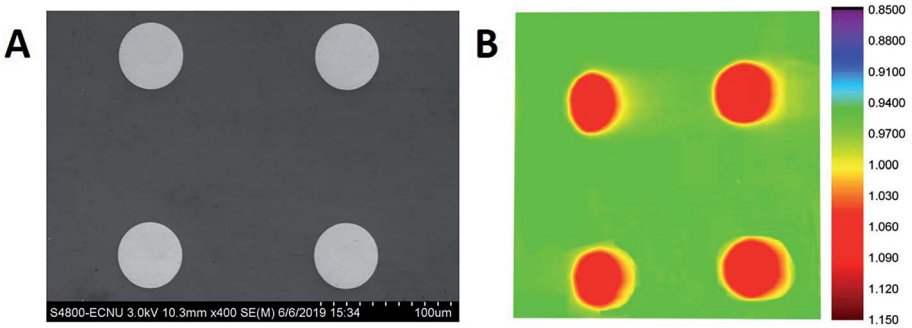

Fig. 2 (A) SEM and (B) SECM images of the gold spot array.

on the relative horizontal position of the tip electrode to the gold spot when the radius of the tip electrode and the tip-to-substrate distance are determined. When the tip electrode is one radius away from the gold spot, the current is completely affected by negative feedback. As it moves to the gold spot, the current increases continuously. When the tip electrode is completely above the gold spot, the current is controlled by completely positive feedback. The relevant current values are calculated, and correlated with the position of the tip electrode, thus obtaining the simulation curves. The experimental curves were plotted by extracting the horizontal cross-sectional lines in the 3D image of the gold spot, thus obtaining the broadening and imaging contrast to calculate the experimental IR values.

The SECM 3D image of the gold spot in Fig. 3A was obtained using a tip electrode with a radius of 12.00 μm, held at a tip–substrate distance of 12.00 μm. To position the tip electrode accurately, the expected tip-to-substrate distance was first substituted into formula (7), generating a current value. When plotting the approach curve over the gold spot, the tip electrode is set to stop at this theoretically calculated current value, and the distance at this moment is the needed value. The experimental curve (Fig. 3D, red solid line) was plotted by extracting the horizontal cross-sectional lines in the 3D image, thus obtaining the broadening and imaging contrast. The experimental IR = 25.23 μm could be calculated according to formula (9) (Table 1). Then, the parameters were substituted into formula (9) for simulation, and the theoretical curve was obtained (Fig. 3D, red dotted line) and the theoretical IR was calculated as 23.03 μm.

Fig. 3B and C show the SECM 3D images obtained using tips with radii of 2.23 μm and 0.76 μm, respectively. The experimental and theoretical curves are also shown in Fig. 3D with the corresponding values of IR listed in Table 1. Obviously, the experimental values are consistent with the theoretical values. Although the experimental and theoretical curves displayed different maximum and minimum values, probably caused by

Table 1 IR obtained using tip electrodes of different radii

a/μm	d/μm	IR (theoretical)/μm	IR (experimental)/μm
12.00	12.00	23.03	25.23
2.23	2.23	4.13	4.93
0.76	0.76	1.46	1.61

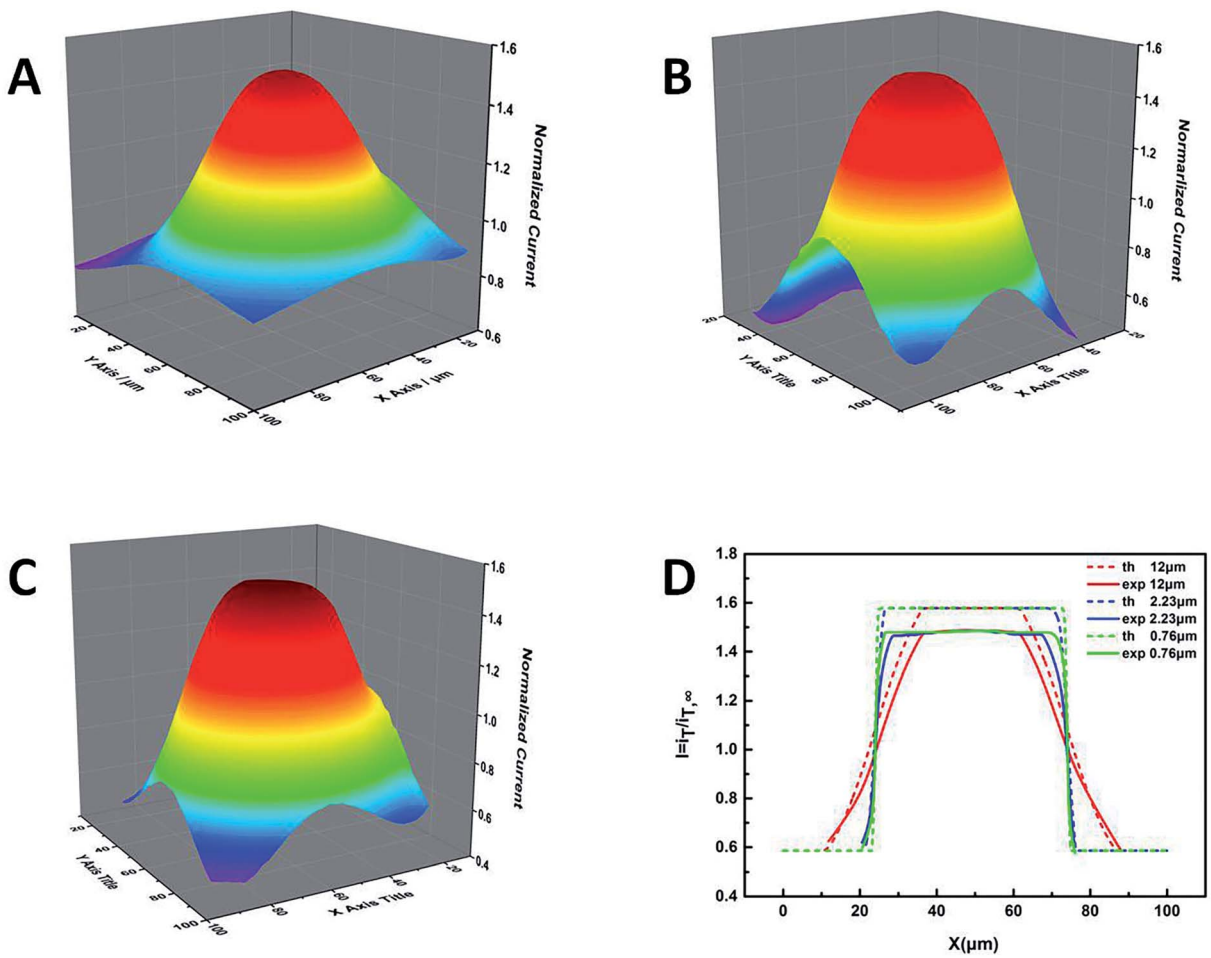

Fig. 3 SECM 3D images of the gold spot obtained using tip electrodes with different radii in 0.1 M KCl containing 0.5 mM FMA solution with holding the potential at +0.45 V: (A) 12.00 μm, (B) 2.23 μm, and (C) 0.76 μm, and (D) the corresponding experimental and theoretical curves.

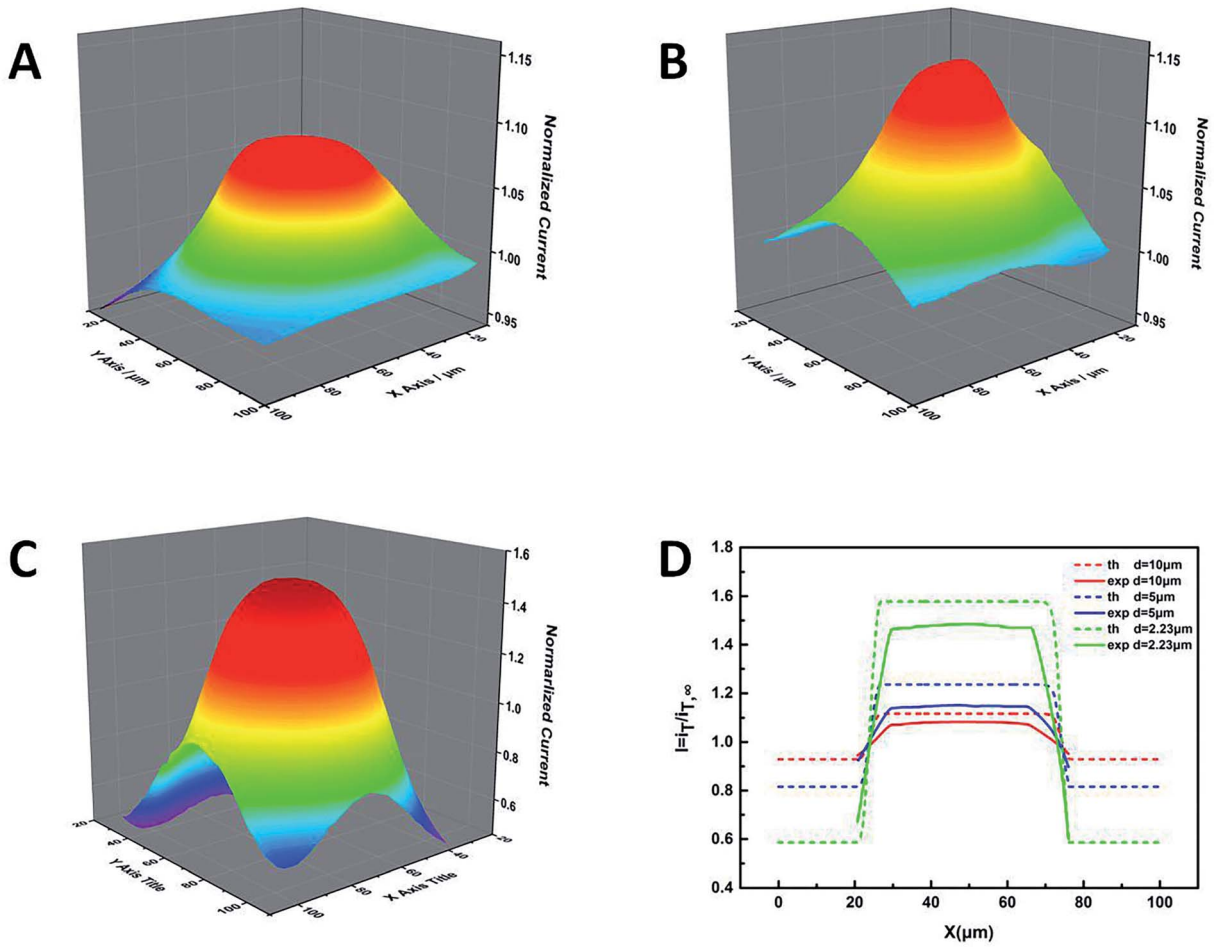

Fig. 4 SECM 3D images of the gold spot at different tip–substrate distances with $E = +0.45$ V in 0.5 mM FMA solution including 0.1 M KCl: (A) 10.00 μm, (B) 5.00 μm and (C) 2.23 μm, and (D) the corresponding experimental and theoretical curves.

the R_G value and forced convection, their similar shapes reveal that by maintaining $d/a = 1$, a higher imaging resolution is obtained using a smaller tip electrode.

Effect of tip–substrate distance on the IR of SECM

The gold spot was scanned by the tip with 2.23 μm radius, when the tip–substrate distance was fixed at 10.00 μm (Fig. 4A), 5.00 μm (Fig. 4B) and 2.23 μm (Fig. 4C), respectively. The alternating conductive and insulating substrate of a sample produces an oscillating curve of normalized current relative to the position.

Because the sample is unbiased, sufficient active substrate area should first be ensured to permit positive feedback, if the value of d/a is large, according to the formulae[31]

$$h^{\infty} = 1 + 1.5L \quad (10)$$

$$L = d/a \quad (11)$$

$$h = a_s/a \quad (12)$$

where a_s is the active radius of the substrate. Herein, $a_s = 25.00$ μm.

So when $a = 2.23$ μm and $d = 10.00$ μm, $L = 4.48$, $h^{\infty} = 7.72$, and $h = 11.20$. Obviously, $h > h^{\infty}$, showing that there is enough active area to allow positive feedback.

Because the size of the tip electrode was fixed, the positive and negative feedback occurred at the same position, but the tip–substrate distance was different. It could be observed that scanning at a smaller tip–substrate distance could generate a larger positive feedback current and a smaller negative feedback current. According to the calculation formula of IR, a smaller value of IR was obtained.

When the tip–substrate distance was 10.00 μm, the IR theoretical value was calculated as IR = 20.65 μm according to formula (9). The experimental IR = 22.87 was approximated to the theoretical value. Also, the IR theoretical and experimental

Table 2 IR obtained with the tip at different tip–substrate distances

a/μm	d/μm	IR (theoretical)/μm	IR (experimental)/μm
2.23	10.00	20.65	22.87
2.23	5.00	9.27	10.74
2.23	2.23	4.13	4.93

values were obtained when the distances were 5.00 μm and 2.23 μm, and shown in Table 2. Clearly, the two groups of values are basically equal.

Fig. 4D shows the variation of the tip current when changing the tip–substrate distance. It could be observed that scanning at a smaller tip–substrate distance could generate a larger positive feedback current and a smaller negative feedback current, thus leading to a larger difference between positive and negative feedback currents, and as a result an improved imaging resolution.

Moreover, the experimental curves presented a similar shape to the theoretical ones. It could be concluded that the higher imaging resolution is contributed by the smaller tip–substrate distance.

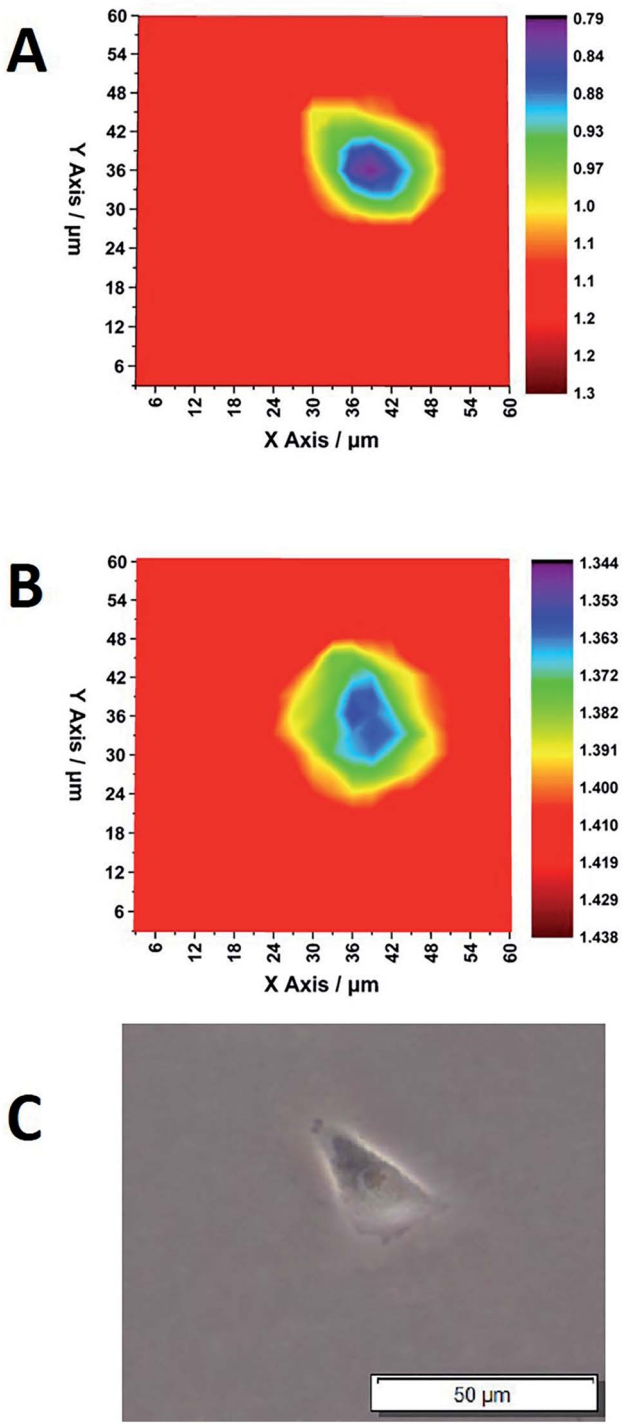

Fig. 5 SECM 2D images of a single cell using tip electrodes at different radii with $E = 0.45$ V in 0.5 mM FMA solution containing 0.1 M KCl: (A) 2.23 μm and (B) 12.00 μm, and (C) optical image of a single cell.

SECM imaging of cells

Human breast cancer cells (MCF-7) were further scanned by two tip electrodes with 12.00 μm (Fig. 5A) and 2.23 μm (Fig. 5B) radii, held at 12.00 μm and 2.23 μm, respectively. Obviously, the cell image obtained with the tip 2.23 μm in radius is closer to the real morphology of the cell with clearer boundaries, further confirming that the tip with a smaller radius could generate smaller IR, thus providing more accurate sample information.

Conclusions

In summary, to discuss the imaging resolution of the boundary between the insulator and the conductor in the feedback mode, the formula of the imaging resolution was proposed, combining the formulae of positive and negative feedback currents. The factors affecting the imaging resolution were investigated. The conclusion is that when the radius of the tip electrode and the tip–substrate distance are the same, the highest imaging resolution can be obtained at a certain tip–substrate distance, and when the radius of the tip electrode is fixed, a smaller tip–substrate distance can generate a higher imaging resolution.

Au disk electrodes of different sizes were fabricated by etched glass encapsulation to verify the accuracy of the imaging resolution formula. The results of gold spot imaging and cell imaging showed that the imaging resolution was indeed related to the radius of the tip electrode and the tip–substrate distance, and the experimental curves were consistent with the simulation curves. This work provides a clearer understanding for the theoretical and experimental studies of SECM imaging resolution.

Conflicts of interest

The authors declare no competing financial interests.

Acknowledgements

This work was financially supported by the National Natural Science Foundation of China (grant no. 21575042).

References

1 A. J. Bard, F.-R. F. Fan, J. Kwak and O. Lev, *Anal. Chem.*, 1989, **61**, 132–138.
2 A. J. Bard, G. Denuault, C. Lee, D. Mandler and D. O. Wipf, *Acc. Chem. Res.*, 1990, **23**, 357–363.
3 R. C. Engstrom, M. Weber, D. J. Wunder, R. Burgess and S. Winquist, *Anal. Chem.*, 1986, **58**, 844–848.

4 N. Arroyo-Curras and A. J. Bard, *J. Phys. Chem. C*, 2015, **119**, 8147–8154.
5 P. Sun and M. V. Mirkin, *Anal. Chem.*, 2006, **78**, 6526.
6 S. Lhenry, Y. R. Leroux and P. Hapiot, *Anal. Chem.*, 2013, **85**, 1840.
7 J. Ufheil, C. Hess, K. Borgwarth and J. Heinze, *Phys. Chem. Chem. Phys.*, 2005, **7**, 3185–3190.
8 M. Shen, R. Ishimatsu, J. Kim and S. Amemiya, *J. Am. Chem. Soc.*, 2012, **134**, 9856–9859.
9 A. G. Marques, J. Izquierdo, R. M. Souto and A. M. Simões, *Electrochim. Acta*, 2015, **153**, 238–245.
10 G. Lu, J. S. Cooper and P. J. McGinn, *Electrochim. Acta*, 2007, **52**, 5172–5181.
11 H. Yamada, D. Haraguchi and K. Yasunaga, *Anal. Chem.*, 2014, **86**, 8547–8552.
12 M. Zhang, Y.-T. Long and Z. Ding, *Chem. Cent. J.*, 2012, **6**, 20.
13 S. Kuss, R. Cornut, I. Beaulieu, M. A. Mezour, B. Annabi and J. Mauzeroll, *Bioelectrochemistry*, 2011, **82**, 29–37.
14 S. Kuss, D. Polcari, M. Geissler, D. Brassard and J. Mauzeroll, *Proc. Natl. Acad. Sci. U. S. A.*, 2013, **110**, 9249–9254.
15 J. M. Liebetrau, H. M. Miller, J. E. Baur, S. A. Takacs, V. Anupunpisit, P. A. Garris and D. O. Wipf, *Anal. Chem.*, 2003, **75**, 563–571.
16 R. T. Kurulugama, D. O. Wipf, S. A. Takacs, S. Pongmayteegul, P. A. Garris and J. E. Baur, *Anal. Chem.*, 2005, **77**, 1111–1117.
17 A. J. Bard and L. R. Faulkner, *Electrochemical Methods: Fundamentals and Applications*, John Wiley & Sons, Inc., New York, 2nd edn, 2000.
18 *Scanning Electrochemical Microscopy*, ed. A. J. Bard and M. V. Mirkin, CRC Press, 2nd edn, 2012.
19 M. V. Mirkin, W. Nogala, J. Velmurugan and Y. X. Wang, *Phys. Chem. Chem. Phys.*, 2011, **13**, 21196–21212.
20 J. Kwak and A. J. Bard, *Anal. Chem.*, 1989, **61**, 1221–1227.
21 J. Kwak and A. J. Bard, *Anal. Chem.*, 1989, **61**, 1794–1799.
22 C. Lee, C. J. Miller and A. J. Bard, *Anal. Chem.*, 1991, **63**, 78–83.
23 F. P. Filice, M. S. M. Li, J. D. Henderson and Z. Ding, *J. Phys. Chem. C*, 2015, **119**, 21473–21482.
24 R. Cornut and C. Lefrou, *J. Electroanal. Chem.*, 2007, **608**, 59–66.
25 C. Lefrou, *J. Electroanal. Chem.*, 2006, **592**, 103–112.
26 C. Lefrou and R. Cornut, *ChemPhysChem*, 2010, **11**, 547–556.
27 A. J. Bard, X. Li and W. Zhan, *Biosens. Bioelectron.*, 2006, **22**, 461–472.
28 Y. Shao and M. V. Mirkin, *J. Phys. Chem. B*, 1998, **102**, 9915–9921.
29 M. V. Mirkin, F. R. F. Fan and A. J. Bard, *J. Electroanal. Chem.*, 1992, **328**, 47–62.
30 Y. Liu, M. Li, F. Zhang, A. Zhu and G. Shi, *Anal. Chem.*, 2015, **87**, 5531–5538.
31 A. J. Bard, M. V. Mirkin, P. R. Unwin and D. O. Wipf, *J. Phys. Chem.*, 1992, **96**, 1861–1868.
32 L. I. Stephens, N. A. Payne, S. A. Skaanvik, D. Polcari, M. Geissler and J. Mauzeroll, *Anal. Chem.*, 2019, **91**, 3944–3950.

